Free Radical Biology & Medicine 51 (2011) 53–68

Contents lists available at ScienceDirect

Free Radical Biology & Medicine

journal homepage: www.elsevier.com/locate/freeradbiomed

Original Contribution

# Cell death via mitochondrial apoptotic pathway due to activation of Bax by lysosomal photodamage

Lei Liu [a], Zhenzhen Zhang [a], Da Xing [a,b,*]

[a] MOE Key Laboratory of Laser Life Science & Institute of Laser Life Science, College of Biophotonics, South China Normal University, Guangzhou 510631, China
[b] Joint Laboratory of Laser Oncology with Cancer Center of Sun Yat-sen University, South China Normal University, Guangzhou 510631, China

ARTICLE INFO

*Article history:*
Received 20 July 2010
Revised 29 March 2011
Accepted 31 March 2011
Available online 8 April 2011

*Keywords:*
Lysosomal photodamage
NPe6–PDT
Bax
Apoptosis
Mitochondrial pathway
Free radicals

ABSTRACT

Lysosomal photosensitizers have been used in photodynamic therapy. The combination of such photosensitizers and light causes lysosomal photodamage, inducing cell death. Lysosomal disruption can lead to apoptosis but its signaling pathways remain to be elucidated. In this study, *N*-aspartyl chlorin e6 (NPe6), an effective photosensitizer that preferentially accumulates in lysosomes, was used to study the mechanism of apoptosis caused by lysosomal photodamage. Apoptosis in living human lung adenocarcinoma cells (ASTC-a-1) after NPe6–photodynamic treatment (NPe6–PDT) was studied using real-time single-cell analysis. Our results demonstrated that NPe6–PDT induced rapid generation of reactive oxygen species (ROS). The photodynamically produced ROS caused a rapid destruction of lysosomes, leading to release of cathepsins, and the ROS scavengers vitamin C and NAC prevent the effects. Then the following spatiotemporal sequence of cellular events was observed during cell apoptosis: Bcl-2-associated X protein (Bax) activation, cytochrome *c* release, and caspase-9/-3 activation. Importantly, the activation of Bax proved to be a crucial event in this apoptotic machinery, because suppressing the endogenous Bax using siRNA could significantly inhibit cytochrome *c* release and caspase-9/-3 activation and protect the cell from death. In conclusion, this study demonstrates that PDT with lysosomal photosensitizer induces Bax activation and subsequently initiates the mitochondrial apoptotic pathway.



Photodynamic therapy is a minimally invasive therapy for cancer treatment, using a photosensitizer and light irradiation [1–3]. Many factors affect its efficacy, one of which being the subcellular localization of the photosensitizer. Researchers therefore have tried to improve the localization of photosensitizers in various cell organelles, including mitochondria, lysosomes, Golgi apparatus, and endoplasmic reticulum (ER) [4–6]. It is generally accepted that the location of the sensitizer coincides with the primary site of photodamage [7–10]. This is because the photogenerated singlet oxygen ($^1O_2$) has a short life and a limited diffusion path in biological systems (half-life <0.04 μs, radius of action <0.02 μm), indicating that primary molecular targets of the photodynamic process must reside within a few nanometers of the photosensitizer [11]. Recently, many lysosomal photosensitizers have been used in photodynamic therapy [1,2]. The combination of light and such photosensitizers causes lysosomal photodamage, inducing cell death. NPe6, a powerful and naturally occurring photosensitizer, preferentially accumulates in lysosomes. Recent reports have shown that irradiation of cells preloaded with NPe6 results in lysosomal disruption, dispersion of lysosomal proteases throughout the cytosol, cleavage/activation of BH3-interacting-domain death agonist (Bid), release of cytochrome *c*, and activation of downstream caspases [12–16]. The mechanism of NPe6–PDT-induced apoptosis is complicated; although activation of Bid has been shown to be involved in the induced apoptosis, other factors, such as Bax, could also play an important role.

Bax, a proapoptotic protein of the Bcl-2 family, is a key regulator of apoptosis. As reported in many apoptotic paradigms, Bax mainly resides in the cytosol of healthy cells, in an inactive state. Upon apoptotic stimulation, Bax undergoes specific conformational changes, integrates into the outer mitochondrial membrane (OMM), and oligomerizes. These oligomers are thought to induce permeabilization of the OMM, allowing the efflux of apoptogenic proteins [17–19]. Consistently, relocation of Bax from the cytosol to the mitochondria has been reported in various photodynamic therapy paradigms to occur with kinetics matching the release of cytochrome *c* [20–22]. The

*Abbreviations:* AIF, apoptosis-inducing factor; Bax, Bcl-2-associated X protein; Bid, BH3-interacting-domain death agonist; CFP, cyan fluorescent protein; ER, endoplasmic reticulum; FACS, fluorescence-activated cell sorter; FRET, fluorescence resonance energy transfer; GFP, green fluorescent protein; $H_2$DCFDA, dichlorodihydrofluorescein diacetate; $LD_{50}$, 50% lethal dose; $LD_{90}$, 90% lethal dose; NAC, *N*-acetylcysteine; NPe6, *N*-aspartyl chlorin e6; OMM, outer mitochondrial membrane; PBS, phosphate-buffered saline; PDT, photodynamic treatment; RFP, red fluorescent protein; RNAi, RNA interference; ROS, reactive oxygen species; $\Delta\Psi_m$, mitochondrial membrane potential.

* Corresponding author at: MOE Key Laboratory of Laser Life Science & Institute of Laser Life Science, College of Biophotonics, South China Normal University, Guangzhou 510631, China. Fax: +86 20 85216052.
*E-mail address:* xingda@scnu.edu.cn (D. Xing).

0891-5849/$ – see front matter © 2011 Elsevier Inc. All rights reserved.
doi:10.1016/j.freeradbiomed.2011.03.042

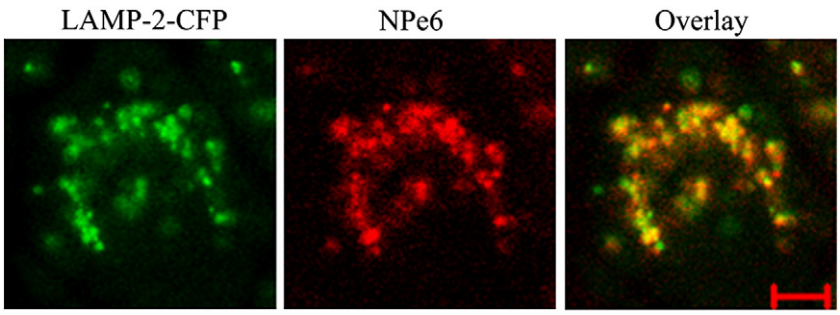


**Fig. 1.** Localization of NPe6 in ASTC-a-1 cells. ASTC-a-1 cells were transfected with LAMP-2–CFP and loaded with NPe6. The fluorescence of LAMP-2–CFP (left) and NPe6 (middle) was visualized by confocal microcopy. The overlay fluorescence image (right) of LAMP-2–CFP and NPe6 indicates that NPe6 is primarily localized in the lysosomes. Scale bar, 10 μm.

extent of Bax involvement in PDT-induced apoptosis depends on a number of factors, including the nature of the photosensitizer and the cell type that is being affected. The apoptotic response of Pc4-mediated PDT was studied in human breast cancer cells (MCF-7c3) treated with Bax antisense oligonucleotides to suppress Bax expression and in the human prostate cancer DU-145 cells, which do not express Bax. In these photosensitized cells the hallmarks of apoptosis, including cytochrome *c* release, caspase activation, and nuclear fragmentation, were inhibited, whereas restoration of Bax expression in DU-145 cells reconstituted these events and precipitated apoptosis [23]. Furthermore, reexpression of mitochondria-targeted Bax is both necessary and sufficient to fully restore caspase activation and apoptotic cell death after hypericin–PDT in apoptosis-deficient $Bax^{-/-}/Bak^{-/-}$ MEF cells [20]. Whether Bax plays an important role in apoptosis induced by lysosomal photodamage is still unknown.

Two separate pathways leading to procaspase activation have been clearly documented: the death receptor-mediated pathway (or extrinsic pathway) and the mitochondria-mediated pathway (or intrinsic pathway) [24,25]. In either pathway, the activation of initiator caspases (caspase-8 or caspase-9) leads to the activation of effector caspases (caspase-3, -6, and -7). The critical role of the mitochondrial pathway in PDT-induced apoptosis has been largely documented [1,2,10]. PDT causes release of mitochondrial apoptogenic proteins into the cytosol, followed by the caspase activation cascade, leading to an apoptotic morphotype. This is especially true for those photosensitizing agents with preferential mitochondrial localization [1,2,7]. Other recent studies have shown that mitochondria are also critical executers of lethal pathways emanating from photodamage to other subcellular sites or organelles [1,2,10,13].

The aim of this study was to investigate the molecular mechanisms of apoptosis induced by lysosomal photodamage. We focused, in particular, on the molecular involvement of Bax in this PDT protocol. By using real-time single-cell analysis, the following events in response to NPe6–PDT were investigated: generation of ROS, disruption of lysosomes, activation of Bax, release of cytochrome *c*, loss of mitochondrial membrane potential ($\Delta\Psi_m$), and activation of caspases.

## Materials and methods

### *Cell culture and transfection*

The human lung adenocarcinoma cell line ASTC-a-1 was obtained from the Department of Medicine, Jinan University (Guangzhou, China) and cultured in DMEM (GIBCO, Grand Island, NY, USA) supplemented with 15% fetal calf serum, penicillin (100 units/ml), and streptomycin (100 mg/ml) in 5% $CO_2$ at 37 °C in a humidified incubator. Transfections were performed with Lipofectamine reagent (Invitrogen, Carlsbad, CA, USA) according to the manufacturer's protocol. The solution of Lipofectamine reagent was replaced with fresh culture medium after 5 h. Cells were examined 36 h after transfection.

### *Photodynamic treatment*

Cells ($1\times10^4$ per well) growing in 35-mm petri dishes were incubated in the dark at 37 °C with 50 μM NPe6 (Light Science Corp., USA) for 1 h. After the culture medium was removed, the cells were rinsed with phosphate-buffered saline (PBS) and then irradiated with a semiconductor laser at 635 nm (NL-FBA-2.0-635, Shanghai, China). The laser light was delivered using an optical fiber (core diameter 400 mm) with a custom distal microlens. The laser power was measured using a laser power meter (FieldMate; Coherent, Santa Clara, CA, USA). The light intensity was set at 2 mW/cm$^2$.

### *Time-lapse confocal fluorescence microscopy*

Cellular GFP, CFP, $H_2$DCFDA, fluorescein isothiocyanate (FITC), rhodamine 123, and MitoTracker red were monitored confocally using a laser-scanning microscope (LSM 510/ConfoCor 2) combination system (Zeiss, Jena, Germany) equipped with a Plan-Neofluar 40×/1.3 NA oil DIC objective. Excitation wavelength and detection filter settings for each of the fluorescent indicators were as follows. GFP, $H_2$DCFDA, FITC, and rhodamine 123 were excited at 488 nm with an

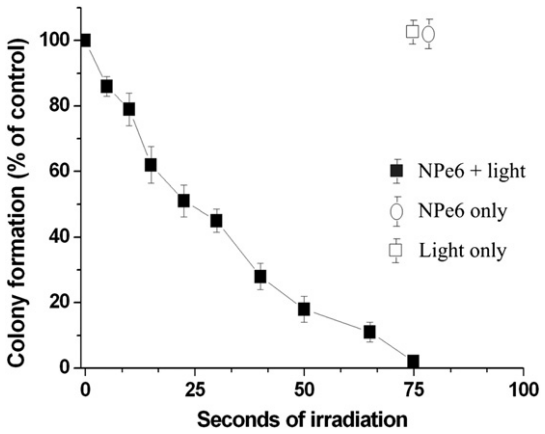


**Fig. 2.** NPe6 cytotoxicity as assessed in colony-forming assays. ASTC-a-1 cells were plated at densities of 500–1200 cells per 60-mm dish. Approximately 24 h later cultures were loaded with 50 μM NPe6 for 1 h before being washed and refed, and then the cells were irradiated. After the indicated times of irradiation, cultures were returned to the incubator. Colonies were counted 8–10 days after irradiation. Data represent means ± SD of three plates per treatment group.

argon ion laser and fluorescence emission was recorded through a 500- to 530-nm IR band-pass filter. CFP was excited at 458 nm with an argon ion laser and its fluorescence emission was recorded through a 470- to 500-nm band-pass filter. MitoTracker red was excited at 633 nm with a He–Ne laser and emitted light was recorded through a 650-nm long-pass filter. For time-lapse imaging, culture dishes were mounted onto the microscope stage equipped with a temperature-controlled chamber (Zeiss).

*Bax translocation assay*

ASTC-a-1 cells were transiently transfected with CFP–Bax (a generous gift from Dr. R.J. Youle of National Institutes of Heath, Bethesda, MD, USA). MitoTracker red was used to label mitochondria. Thirty-six hours after transfection, live cell imaging was performed using the Zeiss LSM 510 confocal microscope at 37 °C. The images of CFP–Bax and MitoTracker red were obtained separately and then merged. The CFP–Bax localization in mitochondria was determined based on the overlap of the CFP–Bax and MitoTracker red fluorescence images.

*Immunofluorescence*

Immunofluorescence for Bax activation was performed as described previously [26]. Briefly, MitoTracker red was added to the medium, and cells were incubated at 37 °C for 30 min. Slides were fixed in 4% paraformaldehyde for 15 min at room temperature and then washed five times with PBS. Samples were incubated in blocking buffer (10% bovine serum albumin in PBS) for 1 h at room temperature, followed by incubation with anti-Bax antibody 6A7 (5 μg/ml in blocking buffer; Abcam, Cambridge, UK) at 4 °C overnight. Cells were washed five times for 5 min each, after which Alexa Fluor 488-conjugated rabbit anti-mouse secondary antibody (diluted 1:400 in blocking buffer; Invitrogen) was added for 1 h at room temperature. After five additional washes with PBS, slides were mounted and analyzed by confocal microscopy.

*RNA interference*

The suppression of Bax, cathepsin B, and cathepsin D was accomplished using small interfering RNA (siRNA) sequences. The sequence of the siRNA specific for Bax was 5′-AACATGGAGCTGCAGAGGATGAdTdT-3′. The sequences of the siRNAs specific for cathepsin B and cathepsin D were 5′-TGAGCTGGTCAACTATGTCdTdT-3′ and 5′-GAACATCTTCTCCTTC-TACdTdT-3′, respectively. A control siRNA specific for the GFP DNA sequence 5′-CCACTACCTGAGCACCCAGdTdT-3′ was used as a negative control. The siRNA sequences were transfected into cells using Lipofectamine reagent (Invitrogen) according to the manufacturer's instructions. In the experiments using siRNAs, the cells were treated with specific siRNA for 48 h first, and then the treated cells were used to perform various experiments as desired.

*Subcellular fractionation*

Cytosolic and mitochondrial fractions were prepared as follows. Cells were harvested, resuspended in 2 pellet volumes of lysis buffer [80 mM KCl, 250 mM sucrose, 50 μg/ml digitonin (Sigma–Aldrich, St. Louis, MO, USA), 1 mM dithiothreitol, and Protease Inhibitor Cocktail Set I (Calbiochem, San Diego, CA, USA)], and placed on ice for 10 min. Samples were centrifuged at 10,000 *g* for 5 min, and cytosol was transferred to new tubes. The pellet was resuspended in wash buffer (20 mM Hepes–KOH and 250 mM KCl) and centrifuged again. To extract mitochondrial proteins, the pellet was resuspended in lysis buffer, lysed by freeze/thaw, and centrifuged at 20,000 *g* for 10 min. The supernatant, containing mitochondrial proteins, and the cytosol were analyzed by Western blot.

Cytosolic and lysosomal fractions were prepared using a lysosomal enrichment kit from Pierce Biotechnology. Cells were harvested and lysed following the manufacturer's instructions. During the entire protocol the samples were kept at 4 °C. The lysates were combined with OptiPrep to a final concentration of 15% and placed on top of a discontinuous density gradient with the following steps from top to bottom: 17, 20, 23, 27, and 30%. After centrifugation for 2 h at 145,000 *g*, the top fraction containing the lysosomes was collected. Other fractions

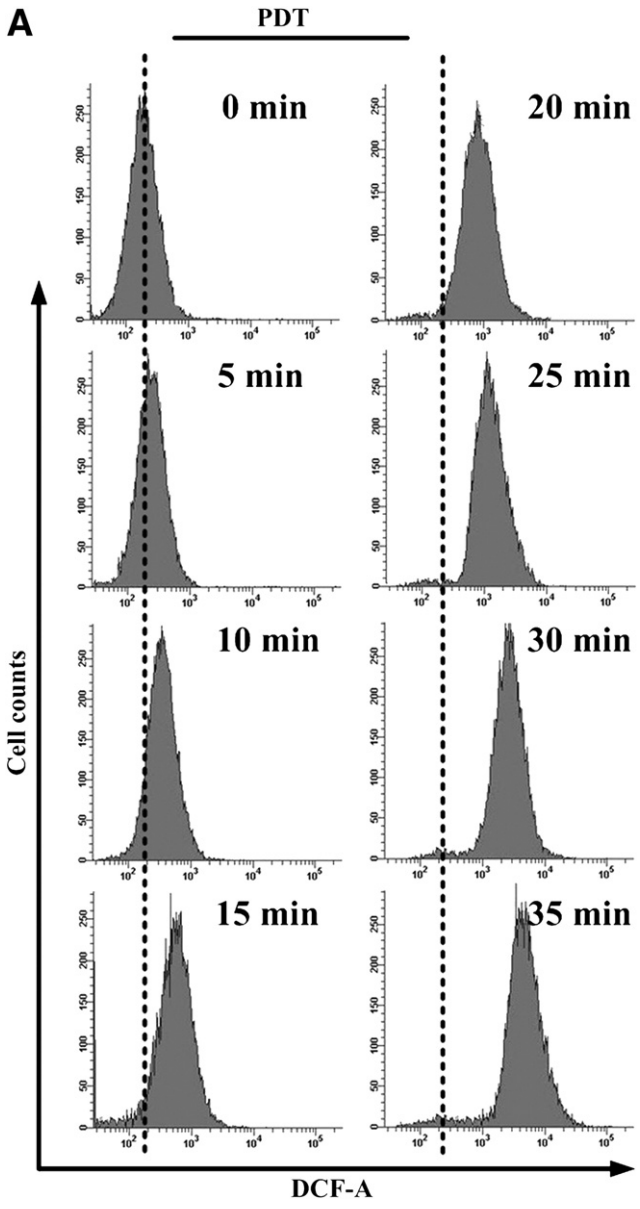


**Fig. 3.** Detection of ROS generation and lysosome integrity in response to NPe6–PDT. (A, B) Detection of ROS generation. After PDT, the samples were stained with $H_2$DCFDA immediately. Then the samples were measured by (A) FACSCanto II cytofluorimeter or (B) fluorescence confocal microscopy. The time points posttreatment are shown in the images. (C) Detection of cathepsin B release using confocal microscopy. The ASTC-a-1 cells were stained with cathepsin B–RFP and LAMP-2–CFP after various treatments as indicated for 1 h. Typical confocal images of cathepsin B–RFP and LAMP-2–CFP are shown separately and their overlay shows the subcellular localization of cathepsin B–RFP. Bar, 5 μm. Similar results were obtained from three independent experiments. (D) Quantification of cells showing cathepsin B release. After various treatments as indicated for 1 h, the percentage of cells showing cathepsin B release into the cytoplasm was assessed by counting the cells exhibiting cytoplasmic cathepsin B. Data represent the means ± SD of three independent experiments; $^{*}p<0.05$ versus untreated group. (E) Detection of cathepsin B and D release using Western blotting analysis. LAMP-2 is a marker for lysosomes, and β-actin for cytosol proteins. Lyso, lysosomes. Similar results were obtained from three independent experiments.

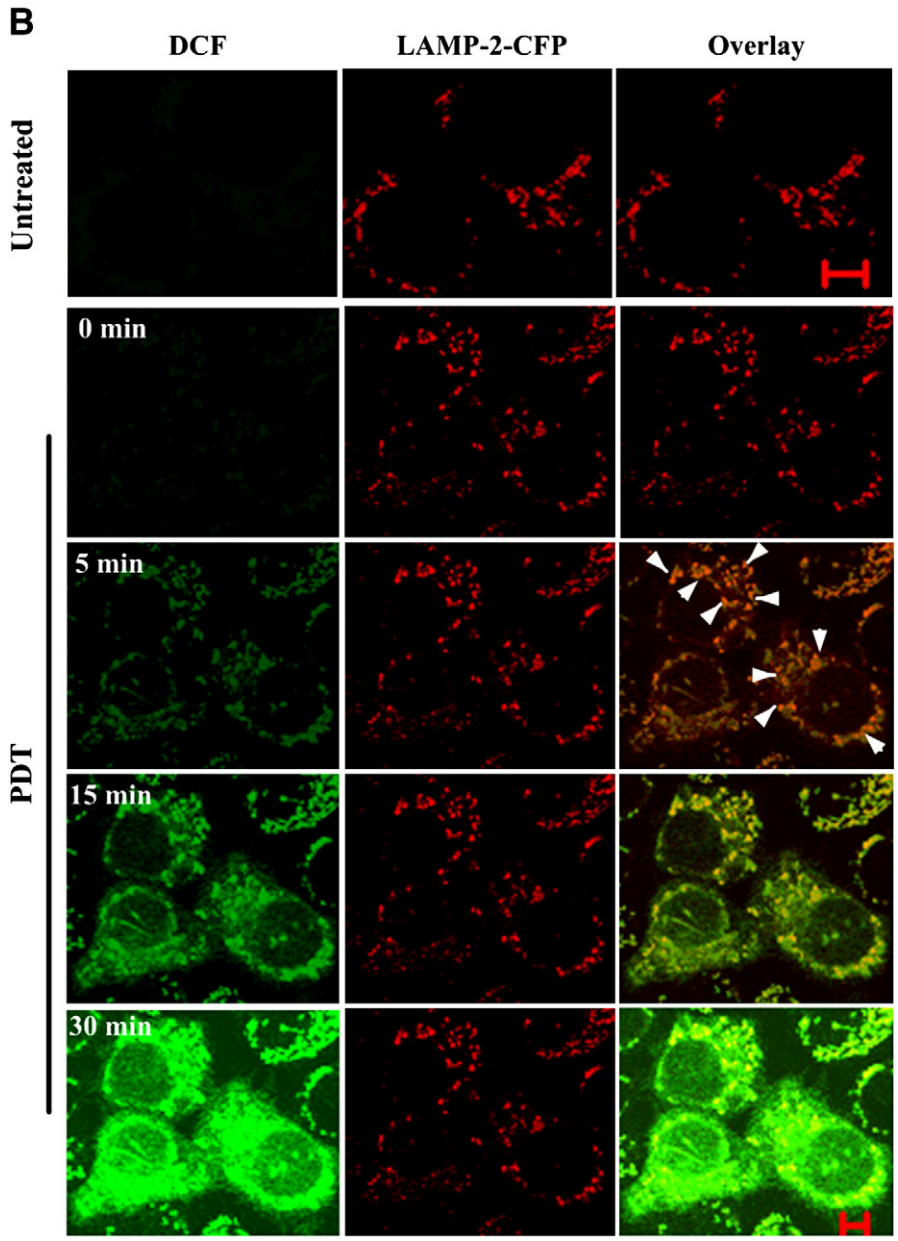


**Fig. 3** (*continued*).

present in the gradient were also collected and combined. Then the collected fractions were analyzed by Western blot.

*Fluorescence-activated cell sorter (FACS) analyses of cell apoptosis*

We used annexin V–FITC (0.1 μg/ml) for the assessment of phosphatidylserine exposure and propidium iodide (0.5 μg/ml) for cell viability analysis. Cell death was measured in a FACSCanto II cytofluorimeter (Becton–Dickinson, Mountain View, CA, USA).

*FACS analyses of $\Delta\Psi_m$*

Rhodamine 123 was used to evaluate the $\Delta\Psi_m$. Cells ($1\times10^5$ per well) growing in petri dishes were loaded with rhodamine 123 and then rinsed three times with PBS before measurement. Leakage from mitochondria was quantified in a FACSCanto II cytofluorimeter.

*Effects of PDT on cell viability*

Subconfluent cultures were trypsinized, washed, and subsequently suspended in culture medium and plated. NPe6 was added 24 h after plating. Then the cultures were washed three times with PBS and refed immediately before irradiation. After irradiation, cultures were returned to the humidified chamber (5% $CO_2$) and incubated at 37 °C. The medium was changed every 3 days and colonies were scored 8–10 days after plating.

*Western blotting analysis*

Western blotting was performed as described previously [27,28]. Briefly, equal amounts of proteins were loaded on SDS/PAGE, transferred to nitrocellulose membranes, and blotted with primary antibodies (Cell Signaling Technology, Danvers, MA, USA) at a dilution of 1:1000,

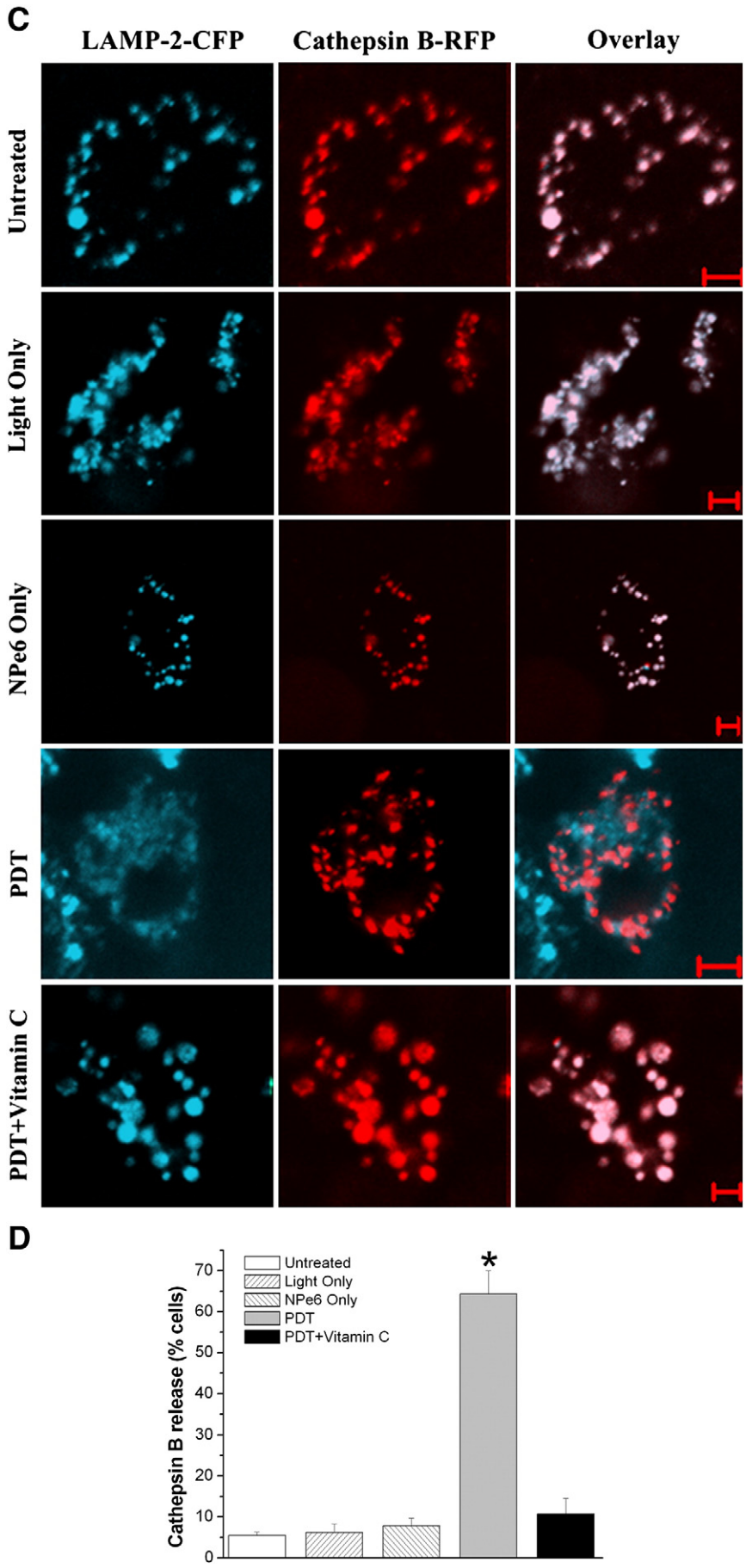


**Fig. 3** (*continued*).

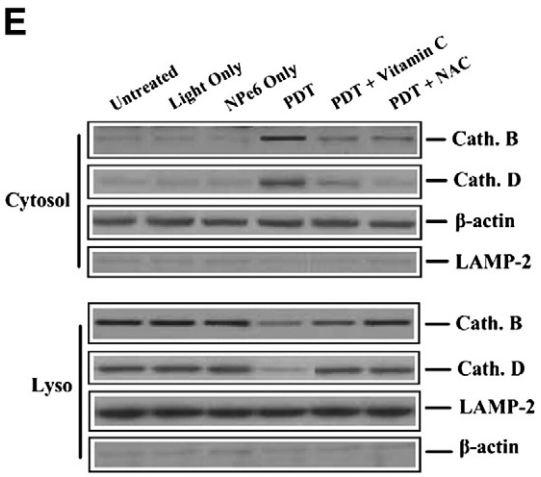


**Fig. 3** (*continued*).

followed by secondary antibodies [goat anti-rabbit conjugated to IRDye 800 (Rockland Immunochemicals, Gilbertsville, PA, USA) or goat anti-mouse conjugated to Alexa Fluor 680 (Invitrogen) for caspase-8]. Detection was performed using the Li-Cor Odyssey scanning infrared fluorescence imaging system (Li-Cor, Lincoln, NE, USA).

### *Image processing and statistical analysis*

To quantify cells showing cytosolic cathepsin B–RFP, ASTC-a-1 cells cotransfected with LAMP-2–CFP and cathepsin B–RFP were subjected to different treatments. At selected time points, the percentage of cells showing cathepsin B–RFP released from lysosomes was assessed by counting the cells exhibiting cytoplasmic cathepsin B–RFP. Data were collected from $n = 150$–$200$ cells per treatment in 10–15 randomly selected image frames from different experiments.

To quantify cells showing mitochondrial CFP–Bax, ASTC-a-1 cells stained with CFP–Bax and MitoTracker red were subjected to different treatments. At selected time points, the percentage of cells showing Bax translocation to mitochondria was assessed by counting the cells exhibiting mitochondrial Bax. Data were collected from $n = 150$–$200$ cells per treatment in 10–15 randomly selected image frames from different experiments.

Experiments were performed in triplicate. Data are represented as means ± SD. Statistical analysis was performed with Student's paired $t$ test. Differences were considered statistically significant at $p < 0.05$.

## Results

### *Intracellular localization of NPe6 in ASTC-a-1 cells*

To determine whether NPe6 localized in lysosomes in ASTC-a-1 cells, LAMP-2–CFP was transfected into cells to label lysosomes and NPe6 was loaded simultaneously. The fluorescence emissions of LAMP-2–CFP and NPe6 were visualized by confocal microcopy, as shown in Fig. 1. In the overlay image, NPe6 fluorescence emission coincided closely with that of LAMP-2–CFP, indicating the lysosomal localization of NPe6 in ASTC-a-1 cells.

### *NPe6–PDT cytotoxicity in ASTC-a-1 cells*

A colony-formation assay was used to determine the cytotoxicity of NPe6–PDT in ASTC-a-1 cells. Cell viability after various treatments as indicated is shown in Fig. 2. Exposure to 50 μM NPe6 alone, in the absence of light, was not cytotoxic to cells. Likewise, light alone, in the absence of photosensitizer, did not affect cell viability. However, irradiation of cells preloaded with NPe6 resulted in light-dose-dependent cell killing (Fig. 2). The $LD_{50}$ and $LD_{90}$ for 50 μM NPe6 were 45 (22.5-s irradiation) and 130 mJ/cm$^2$ (65-s irradiation), respectively. In subsequent PDT studies, unless stated otherwise, cells were treated with 50 μM NPe6 and 130 mJ/cm$^2$.

### *ROS generation and lysosome disruption*

To monitor ROS generated by NPe6–PDT, the fluorescent product DCF was determined by confocal microscopy and flow cytometry. The samples were treated with PDT and then loaded with $H_2$DCFDA immediately. The treated samples were analyzed at the indicated time points. The results show that PDT induced rapid generation of ROS, which increased with time (Figs. 3A and B).

As shown in Fig. 1, NPe6 preferentially accumulates in the lysosomes; hence the immediate generation of ROS is anticipated to occur in the lysosomes. To clarify this issue, LAMP-2–CFP was transfected into cells to label lysosomes, and $H_2$DCFDA was loaded to monitor the ROS generation; the fluorescence of LAMP-2–CFP and DCF was visualized by confocal microcopy. It was observed that ROS were generated rapidly after PDT; the arrows in the overlay image show that ROS first appear in lysosomes (Fig. 3B).

We further investigated whether the generation of ROS affected the integrity of lysosomes. The fluorescence confocal images were utilized to monitor the dynamic behavior of cathepsin B, a lysosomal protease. The fusion protein cathepsin B–RFP was utilized to follow cathepsin B migration, and LAMP-2–CFP was utilized to label the lysosomes. Typical images of cathepsin B–RFP distribution after various treatments are shown in Fig. 3C. The data showed that

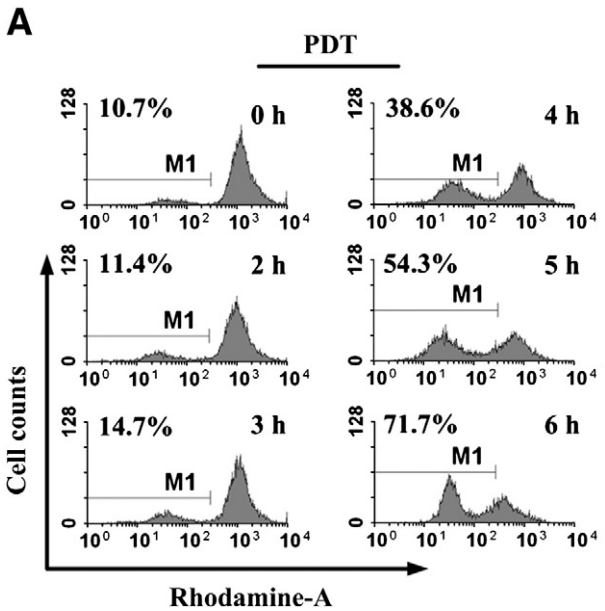


**Fig. 4.** Effects of NPe6–PDT on mitochondrial apoptotic pathway. (A) Effects of NPe6–PDT on $\Delta\Psi_m$. The samples were labeled with rhodamine 123 and then treated with PDT. The samples were measured by FACSCanto II cytofluorimeter at the indicated time points. Similar results were obtained from four independent experiments. (B) Detection of cytochrome *c* release. (C) Caspase-9 activation. (D) Caspase-3 activation. The samples were treated as indicated. Cell lysates were subjected to immunoblotting. β-Actin served as a loading control. For (B) to (D), densitometric results of three separate blots were used for quantitative analysis. For densitometry, values were normalized according to the control sample lanes, which were arbitrarily set as 1; data represent means ± SD.; $^*p < 0.05$ versus untreated group.

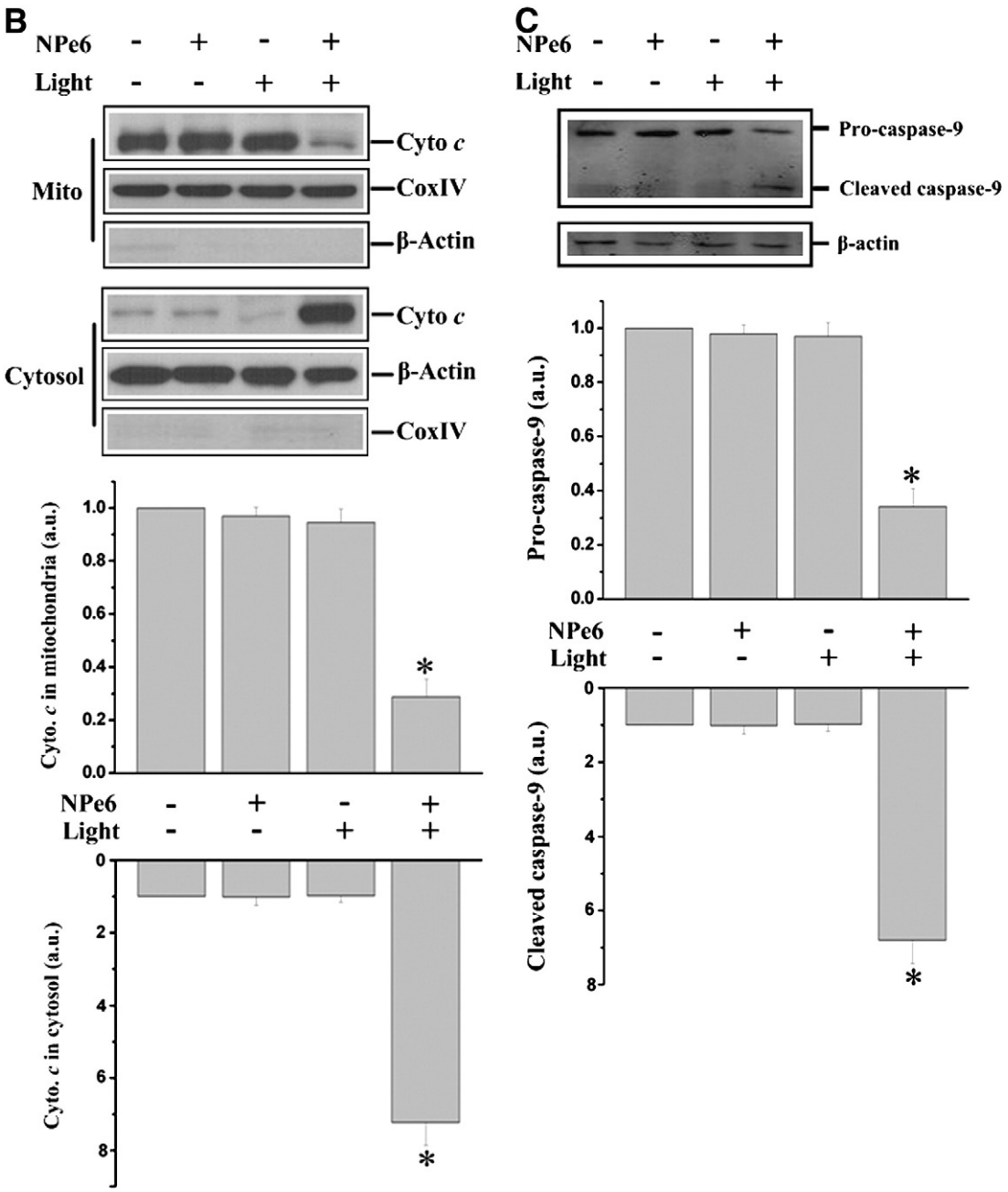


**Fig. 4** (*continued*).

cathepsin B was localized in lysosomes in the untreated group; exposure to light or to NPe6 alone did not affect its subcellular localization. PDT induced cathepsin B redistribution to cytosol, and the addition of vitamin C, a ROS scavenger, could inhibit this process. Most of the cells were subjected to cathepsin B release after PDT (Fig. 3D). Furthermore, Western blotting results also clearly showed that NPe6–PDT induced cathepsin B and cathepsin D release into the cytosol, and vitamin C and NAC could prevent this release (Fig. 3E). These results suggested that the ROS induced by NPe6–PDT triggered a rapid destruction of lysosomes.

*Activation of mitochondrial apoptotic pathway in response to lysosomal photodamage*

To assess the involvement of the intrinsic pathway of apoptosis induced by NPe6–PDT, we examined the integrity of the mitochondria. Rhodamine 123 is a fluorescent probe used to monitor $\Delta\Psi_m$. Cells were preloaded with rhodamine 123 and treated with NPe6–PDT, and then the cells were tested using flow cytometry. The results showed that the $\Delta\Psi_m$ decreased dramatically at about 4 h after PDT and continued to decrease with time (Fig. 4A).

Cytochrome *c* release from mitochondria is a critical step in the mitochondrial apoptotic pathway. Western blotting results showed that exposure to NPe6 alone or exposure to light alone did not release cytochrome *c* from mitochondria. However, PDT resulted in cytochrome *c* release from mitochondria to the cytosol (Fig. 4B). This result was also confirmed by monitoring the dynamic behavior of cytochrome *c* in living cells using confocal microscopy (see Supplementary Fig. 1A). Before cytochrome *c* release, the distribution patterns of both cytochrome *c* and MitoTracker red were the same as that of mitochondria, appearing as filamentous structures as shown in the untreated cell. PDT resulted in cytochrome *c* release from

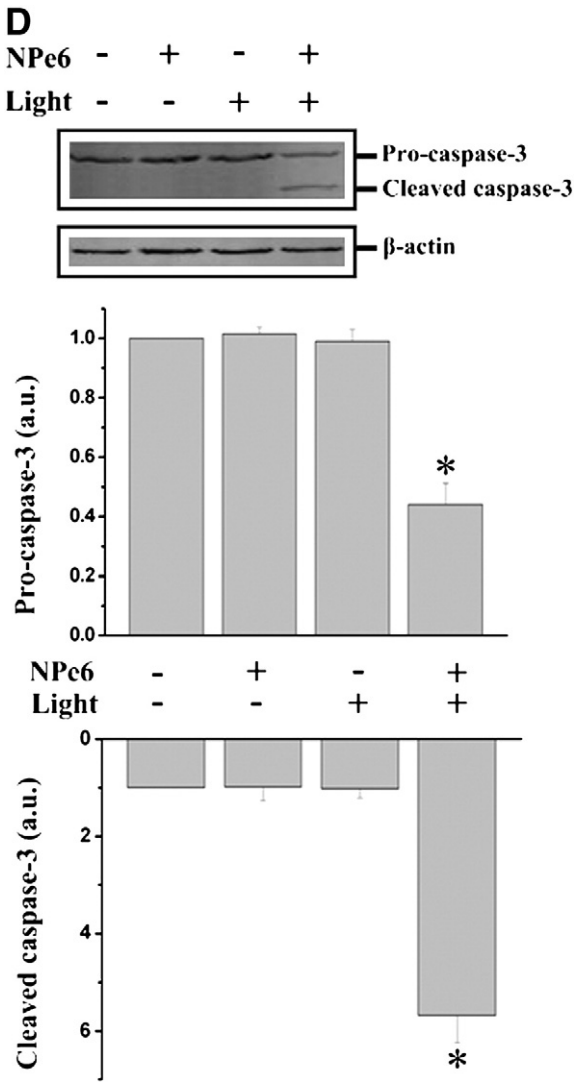


**Fig. 4** (*continued*).

mitochondria, as shown by the overlay image, in which cytochrome *c* displayed a diffuse and cytoplasmic localization. Our results showed that most of the cells were subjected to cytochrome *c* release after PDT (see Supplementary Fig. 1B).

Cytochrome *c* release can activate a downstream caspase cascade, which is a key event during apoptosis. To determine whether caspases were activated, we measured the changes in caspase-9 and caspase-3 activities in response to NPe6–PDT using Western blot analysis. As shown in Figs. 4C and D, neither irradiation alone nor exposure to NPe6 alone activated procaspase-9 or procaspase-3, whereas NPe6–PDT resulted in cleavage of procaspase-9 and procaspase-3, generating the activated fragment.

The FRET technique was used to analyze dynamic changes in caspase-9 and caspase-3 in living cells (see Supplementary Fig. 2). ASTC-a-1 cells expressing SCAT9 FRET fluorescent reporters were treated as indicated. The control cells (see Supplementary Fig. 2A) showed no change during the recording time. After PDT, caspase-9 activation was indicated by increased emission in the CFP channel and decreased emission in the FRET channel (see Supplementary Fig. 2B). The ratio of FRET/CFP was plotted as a function of time after PDT (see Supplementary Fig. 2C). The fluorescence intensity of FRET/CFP decreased slightly during the first 150 min and then decreased dramatically. About 240 min after PDT, the fluorescence intensity reached a low, stable level. These results indicated that the caspase-9 activity increased gradually from PDT, noticeably 150 min after treatment. The same methods were also used to study whether caspase-3 was activated after PDT. The results showed that caspase-3 activity was also significantly increased after PDT (see Supplementary Fig. 3).

Thus in our experimental model, the typical apoptotic hallmarks, including $\Delta\Psi_m$ decrease, cytochrome *c* release, and caspase-9/-3 activation, suggested that lysosomal photodamage induces cell death via the mitochondrial apoptotic pathway.

### *Real-time detection of Bax activation*

To observe the dynamic redistribution of Bax during NPe6–PDT-induced apoptosis in ASTC-a-1 cells, we utilized the CFP–Bax fusion protein to follow Bax migration with fluorescence imaging. Mito-Tracker red was utilized to label mitochondria. Real-time monitoring of Bax translocation was performed with the laser-scanning microscope.

Typical images of the real-time distribution of CFP–Bax in nonapoptotic control cells are shown in Fig. 5A. CFP–Bax had a diffuse distribution throughout the cytoplasm, with little or no evident association with mitochondria. Fig. 5B ($LD_{90}$ conditions) shows the representative spatial and temporal relationships of CFP–Bax and MitoTracker red after NPe6–PDT. CFP–Bax displayed a diffuse and cytoplasmic localization at the beginning of the treatment. About 100 min posttreatment, CFP–Bax partially translocated to mitochondria from the cytoplasm as revealed by the overlaps of CFP–Bax and MitoTracker red fluorescence images. The majority of CFP–Bax was localized in mitochondria about 150 min posttreatment, as confirmed by the overlay images (Fig. 5B). The experiments performed using $LD_{50}$ conditions also showed Bax translocation to mitochondria (Fig. 5C). Quantification results also showed that PDT induced Bax translocation to mitochondria in most of the treated cells (Fig. 5D).

To further confirm the results obtained from the real-time single-cell analysis, a time course of Bax relocation from the cytosolic fraction to the mitochondrial fraction was investigated by Western blotting analysis after subcellular fractionation. As shown in Fig. 5E, the protein levels of Bax decreased in the cytosolic fraction and, concomitantly, increased in the mitochondrial fraction of ASTC-a-1 cells after NPe6–PDT. Bax can translocate to other intracellular organelles to trigger apoptotic signals in response to apoptotic stimulation. Herein we examined whether Bax translocates to the ER or lysosomal membrane after NPe6–PDT. The Western blotting

**Fig. 5.** Spatial and temporal changes in Bax subcellular localization. (A–C) Typical time-lapse confocal images of living ASTC-a-1 cells stained with CFP–Bax and MitoTracker red under various treatment conditions. The images of CFP–Bax and MitoTracker red are shown separately and their overlay shows the localization of CFP–Bax in mitochondria. (A) Control cells without Bax translocation over time. (B) Time-lapse images of CFP–Bax redistribution after NPe6–PDT under $LD_{90}$ conditions. (C) Time-lapse images of CFP–Bax redistribution after NPe6–PDT under $LD_{50}$ conditions. Similar results were obtained from three independent experiments. Bar, 5 μm. (D) Quantification of cells showing mitochondrial Bax. After various treatments as indicated for 4 h, the percentage of cells showing Bax translocation was assessed by counting the cells exhibiting mitochondrial Bax. Data represent means ± SD of three independent experiments; $^*p<0.05$ versus untreated group. (E) Time course of Bax relocation from the cytosolic fraction (Cytosol) to the mitochondrial fraction (Mito). β-Actin and CoxIV were used as loading controls. Densitometric results of three separate blots were used for quantitative analysis. For densitometry, values were normalized according to the sample lanes at 0 h, which were arbitrarily set as 1; data represent means ± SD; $^*p<0.05$ versus control sample (0 h). (F) Detection of the activation of endogenous Bax. After various treatments as indicated, the cells were fixed and subjected to immunofluorescence staining for active Bax by using a conformation-specific anti-Bax monoclonal antibody (6A7), which could selectively recognize the activated form of Bax. Similar results were obtained from three independent experiments. Bar, 5 μm.

results show that, after NPe6–PDT, Bax translocated to mitochondria obviously, with little or no association with lysosomal or ER membranes (see Supplementary Fig. 4).

To directly detect the activation of endogenous Bax, cells were fixed and subjected to immunofluorescence staining for active Bax using a conformation-specific anti-Bax monoclonal antibody (6A7),

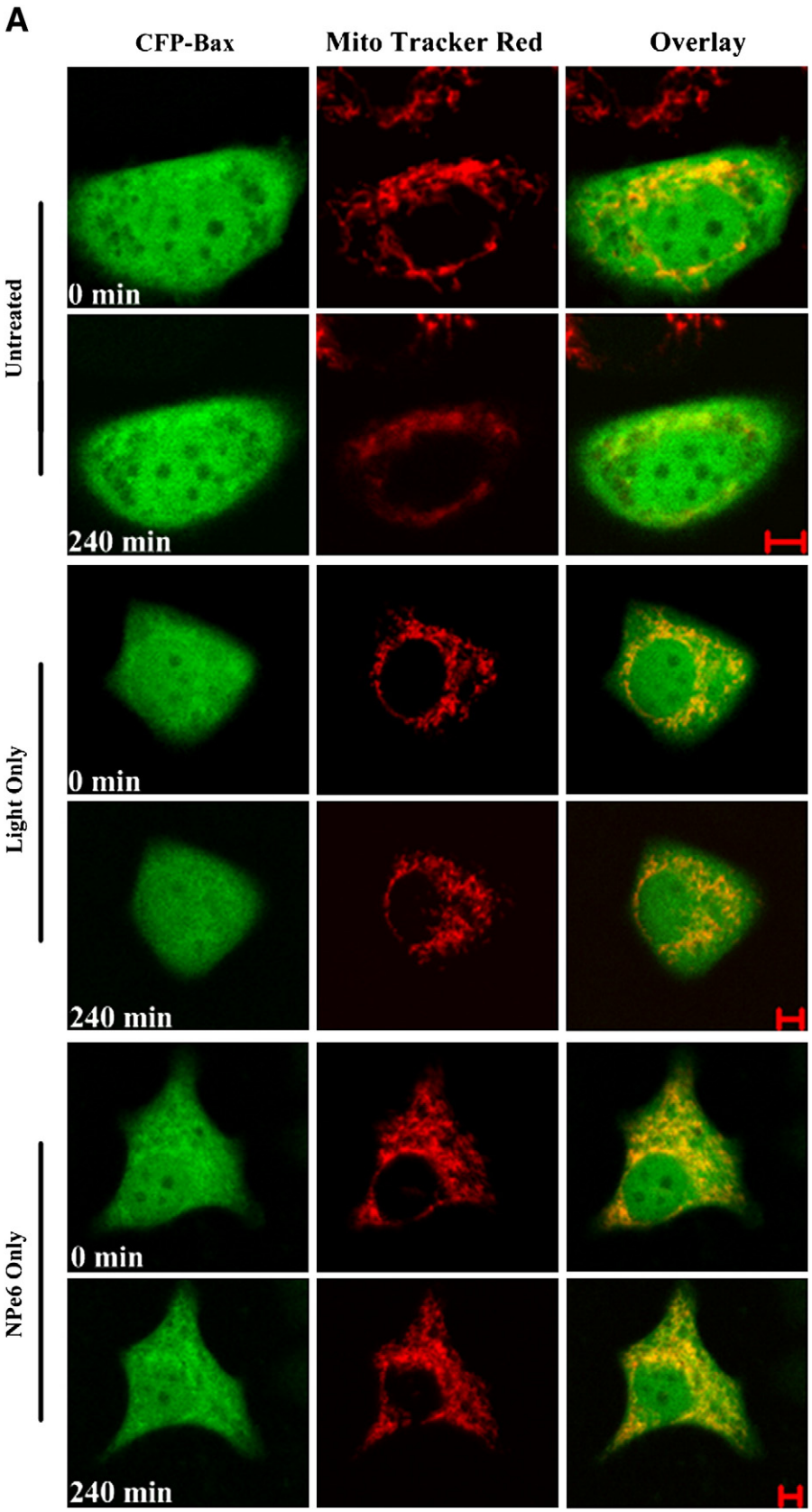

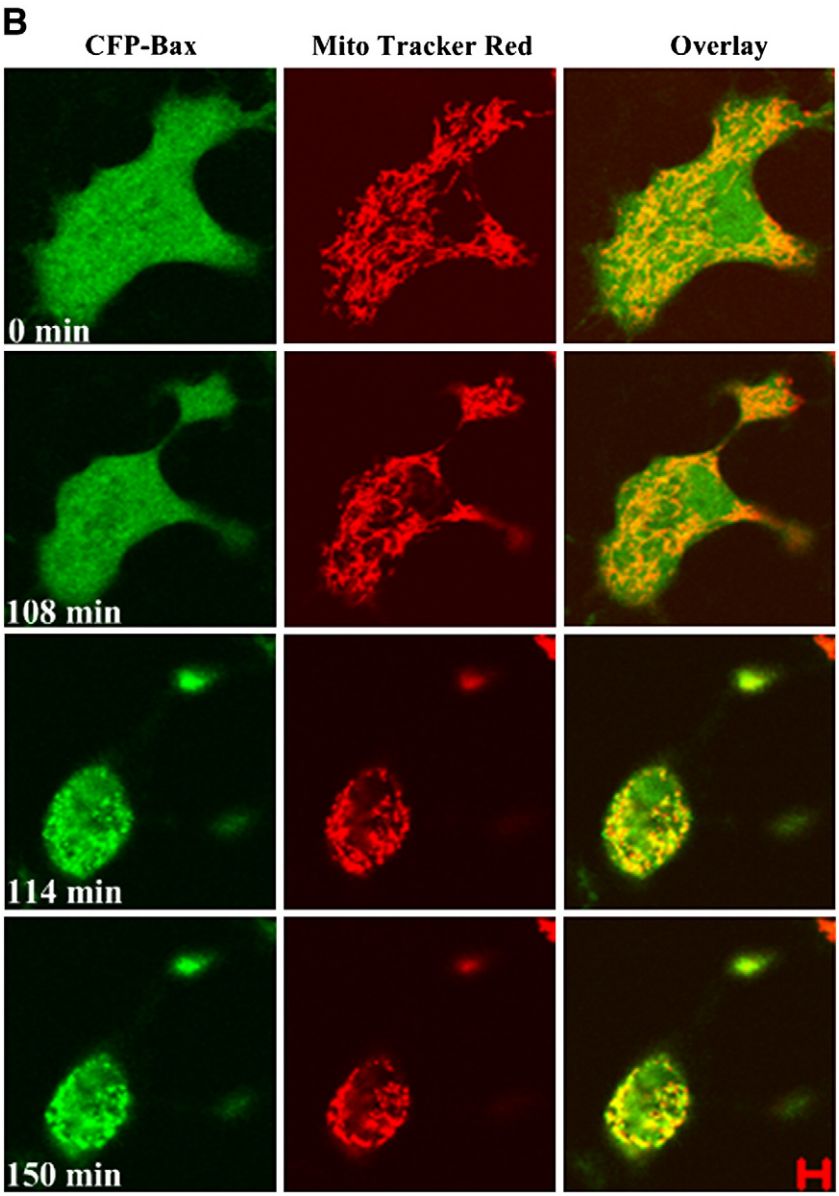


**Fig. 5** (*continued*).

which could selectively recognize the activated/proapoptotic form of Bax. As shown in Fig. 5F, neither irradiation alone nor NPe6 alone caused Bax activation. However, when they were used in combination, Bax was activated and localized in mitochondria (Fig. 5).

*Role of cathepsin D and cysteine cathepsins in Bax activation*

Lysosomes contain numerous proteolytic enzymes, including the aspartic protease cathepsin D and several cysteine proteases (e.g., cathepsin B and L). These lysosomal proteases may play a role in the activation of apoptotic signals. Herein we performed experiments to examine whether these proteases were involved in Bax activation in our experimental model. In our experiments, Z-FA-FMK (a potent, irreversible inhibitor of cathepsin B and L) and pepstatin A (a potent inhibitor of cathepsin D) were used; SiRNA-Cath B and SiRNA-Cath D were also used to silence cathepsin B and cathepsin D, respectively. As the results show (see Supplementary Fig. 5), transfection of siRNA sequences specifically suppressed the expression levels of cathepsin B and cathepsin D. Then we determined the roles of cathepsin B and cathepsin D in Bax activation. As shown in Fig. 6, Z-FA-FMK and SiRNA-Cath B had little effect on Bax translocation to mitochondria, whereas pepstatin A and SiRNA-Cath D could reduce Bax redistribution significantly. These results suggest that cathepsin D plays an important role in Bax activation in NPe6–PDT-induced apoptosis.

*Effects of suppressing Bax on cell apoptosis induced by NPe6–PDT*

Our experiments demonstrated that Bax was activated. To determine whether Bax was indeed an essential component of the death pathway triggered by lysosomal photodamage, we used RNAi to silence the expression of Bax. The data show that the endogenous Bax protein level was significantly down-regulated (>90%) in siRNA-transfected cells (Fig. 7A). Then, we investigated whether suppressing Bax could inhibit the apoptotic signal and protect cells from death. Western blotting results showed that the hallmarks of apoptosis, including cytochrome *c* release (Fig. 7B), caspase-9 activation (Fig. 7C), and caspase-3 activation (Fig. 7D), were significantly inhibited by knockdown of Bax. Statistical analysis

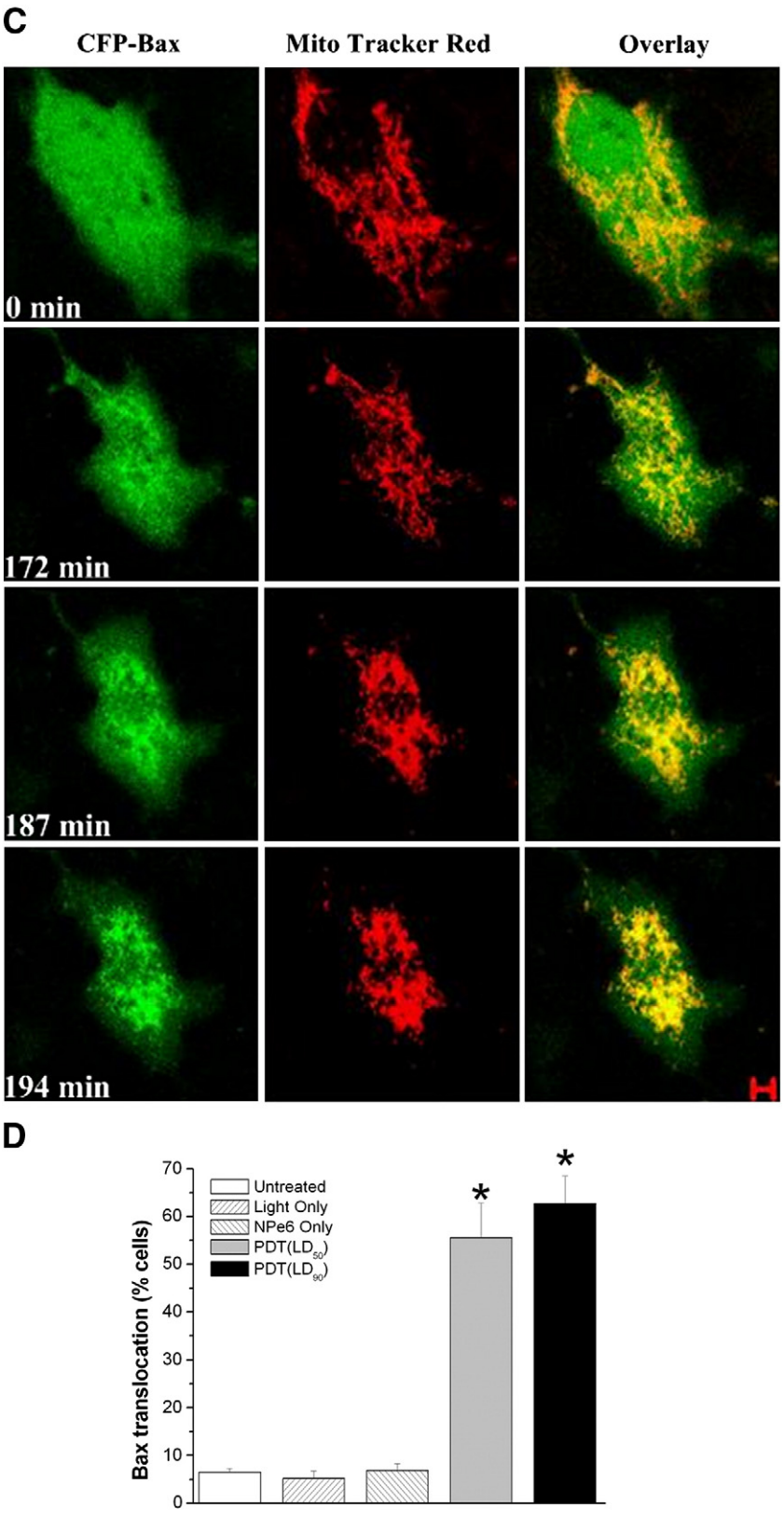


**Fig. 5** (*continued*).

revealed that the cells with down-regulated Bax were resistant to apoptosis induced by PDT (Fig. 7E). These findings demonstrate that Bax plays a crucial role in cell apoptosis induced by lysosomal photodamage.

## Discussion

NPe6–PDT has been shown to be effective in several experimental animal models. Previous studies have shown that NPe6 preferentially

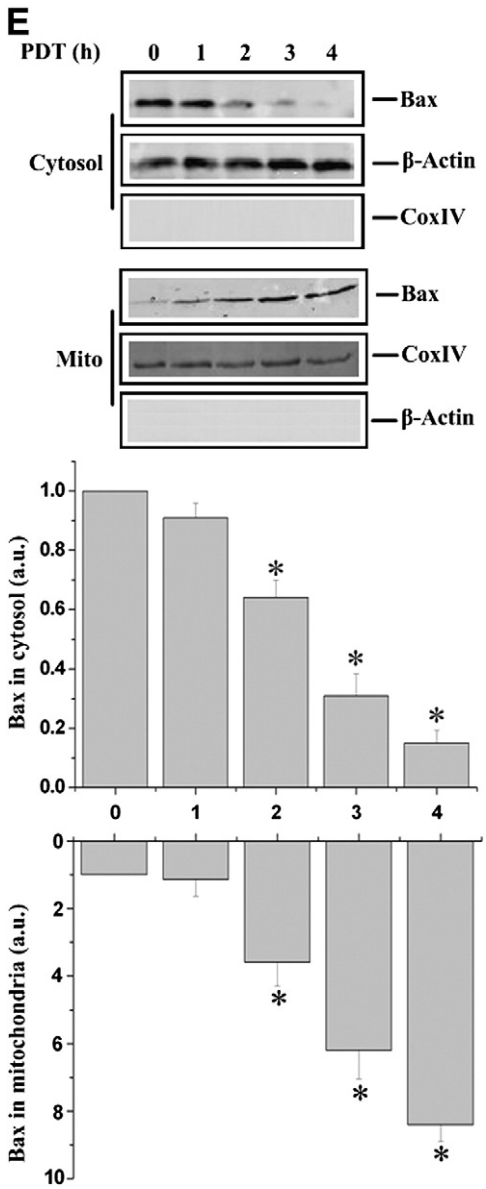


**Fig. 5** (*continued*).

accumulates in lysosomes and causes lysosomal disruption after laser irradiation, resulting in cytochrome *c* release and activation of caspases [12–16]. However, it is not clear how cellular signaling from lysosomal disruption leads to apoptosis. Previous studies suggested that Bid may be involved in apoptosis induced by lysosomal photodamage [13,16]. Results obtained from some other experimental models suggested that lysosomal proteases can directly activate caspases [29,30]. However, our observations are not consistent with a model entailing direct lysosomal protease activation of procaspases. Herein, for the first time, we found that PDT with the lysosomal photosensitizer NPe6 induces Bax activation and subsequently initiates the mitochondrial apoptotic pathway, resulting in caspase activation and cell death. The findings contribute to the understanding of the mechanisms involved in proapoptotic signaling mediated by lysosomal photosensitizer-based PDT.

During apoptosis, engagement of the mitochondrial pathway involves the permeabilization of the OMM, which leads to the release of cytochrome *c* and other apoptogenic proteins such as Smac/DIABLO, AIF, EndoG, and Omi/HtraA2. The OMM permeabilization is controlled by the Bcl-2 family proteins, especially by activation, translocation, and oligomerization of proapoptotic proteins such as Bax and Bak [17–19]. Recently, Bax translocation from the cytosol to the mitochondria as a trigger of OMM permeabilization and apoptogenic proteins release in PDT has been reported [20–22]. However, how and to what extent Bax contributes to apoptosis induced by lysosomal photodamage is still unknown. In this study, using real-time single-cell analysis, we found that 2–3 h after NPe6–PDT, Bax in treated cells started to translocate to mitochondria and, within 30 min, sequestered into clusters (Fig. 5). Knocking down Bax using siRNA could significantly inhibit cytochrome *c* release and caspase-9/-3 activation, hence preventing cell death (Fig. 7). These results demonstrated that activation of Bax plays an important role in apoptosis induced by lysosomal photodamage. Some previous studies have shown that the apoptotic gateway proteins Bax and Bak can translocate to the ER to maintain a homeostatic concentration of $Ca^{2+}$ and regulate cell death initiated by ER stress [31,32]. Other papers have mentioned that Bax can be translocated to the lysosomal membrane in response to apoptotic stimulation and promote the release of lysosomal enzyme to the cytosol to trigger the apoptotic signal [33,34]. Because many photosensitizers accumulate in lysosomal and ER membranes and these compartments are highly susceptible to oxidation, the participation of Bax in regulating these organelle functions in response to PDT could play a more general role. In this study, we examined whether Bax translocated to the ER or lysosomal membranes to trigger the apoptotic signal in response to NPe6–PDT. The results show that, after NPe6–PDT, Bax translocated to mitochondria obviously, with little or no association with lysosomal or ER membranes (see Supplementary Fig. 4).

During apoptosis, the translocation and oligomerization of Bax are central events. However, the mechanism for recruitment of Bax to intracellular organelles is not fully understood. Emerging experimental evidence has shown that BH3-only proteins, such as Bid and Bim, could activate Bax directly or indirectly [19,35–37]. Bidere et al. [38] and Castino et al. [39] reported that cathepsin D was a potential activator of Bax. Chipuk et al. reported that p53 could activate Bax, like Bid and Bim, through direct or indirect pathways [40,41]. Several studies showed that the cleavage of Bax by calpain removed the first 33 amino acids of the N-terminal, resulting in the activation of Bax [42,43]. Considering that NPe6–PDT triggers lysosomal disruption and results in protease efflux, in this study, we investigated whether cathepsins were involved in cell apoptosis induced by NPe6–PDT. The results suggest that cathepsin D plays an important role in Bax activation in NPe6–PDT-induced apoptosis, whereas cysteine proteases, such as cathepsin B and L, have little or no effect on Bax activation (Fig. 6). Further studies are needed to explored the mechanisms by which cathepsin D modulates Bax activation.

The ROS produced during PDT have been shown to destroy tumors by multifactorial mechanisms [10,44,45]. Because singlet oxygen has a short lifetime in cells, its intracellular targets are located close to the sensitizer [11]. Therefore, the subcellular location of a photosensitizer critically influences the kinetics and the regulatory pathway activated by PDT [7–9]. Thus it is not surprising that PDT with mitochondrial photosensitizers can induce apoptosis rapidly [7]. However, because photosensitizers may also be accumulated in other cellular compartments (e.g., lysosomes, ER, or Golgi apparatus), local damage induced by photosensitization may be propagated to the mitochondria. Many reports have shown that oxidative damage to the ER after PDT can result in dramatic changes in ER homeostasis, which can be further propagated to the mitochondrial cell death machinery [1,2,4,10]. PDT with the photosensitizer NPe6 promoted Bid cleavage and triggered the mitochondrial pathway through the release of cathepsins in response to lysosomal photodamage [12–16]. The signaling mechanisms transducing the primary photodamage to the lysosomes into cell death pathways in cells after NPe6–PDT are not completely

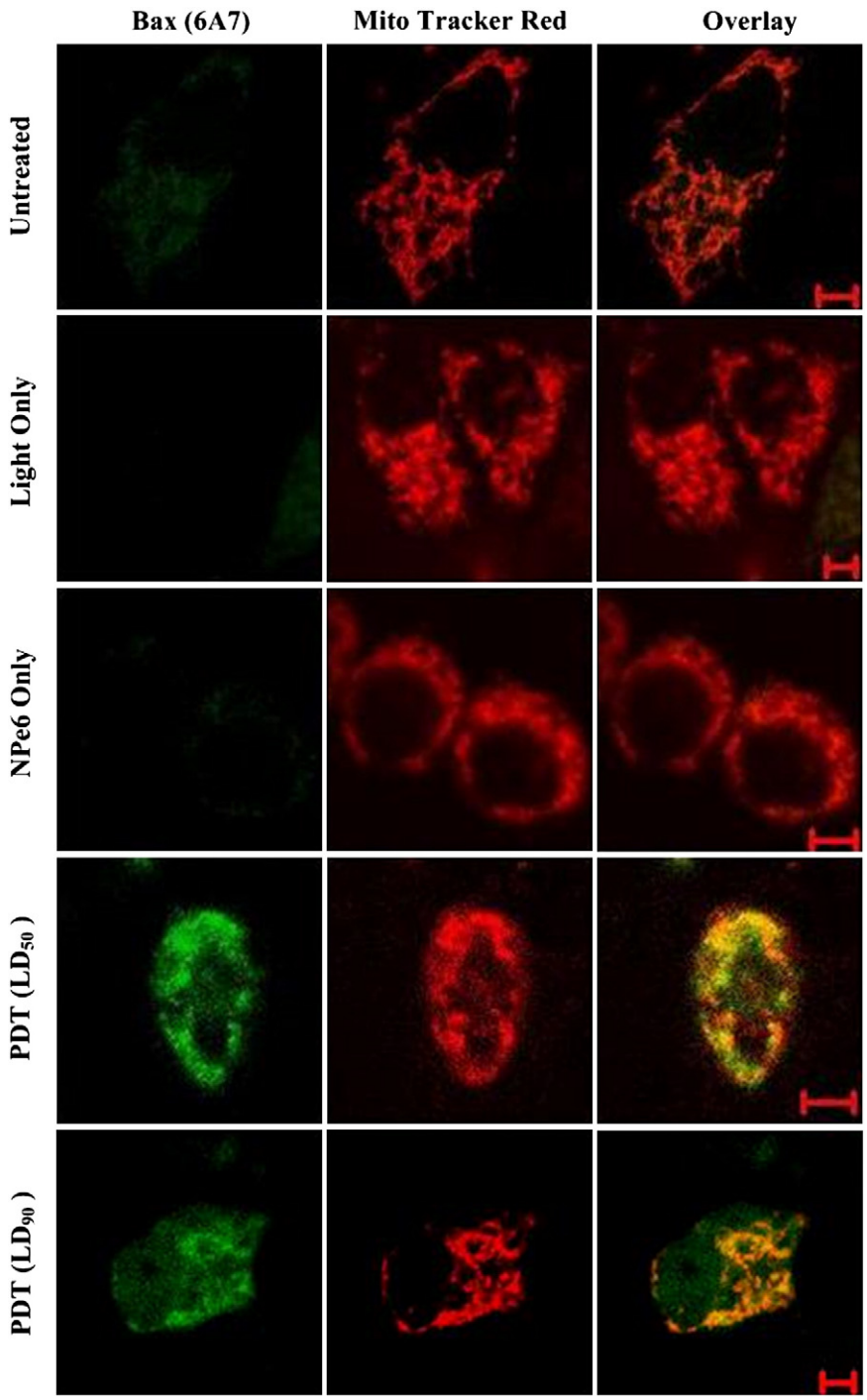


**Fig. 5** (*continued*).

delineated, but a role for the activation of Bax, which mediated the mitochondrial apoptotic pathway, has been proposed in this study.

Caspases are present in mammalian cells as inactive protease precursors (procaspases) and are classified as upstream initiator caspases (caspase-8 and -9) and downstream effector caspases (such as caspase-3, -6, or -7). Caspase-8 and -9 are first activated in response to apoptotic stimuli and are responsible for processing and activating the extrinsic pathway and the intrinsic pathway, respectively [24,25]. In our previous study, we found that lysosomal photodamage could not induce the activation of caspase-8 [16]. Here, by using the FRET technique, the dynamic activation of caspase-9 and caspase-3 induced by lysosomal photodamage was detected (see Supplementary Figs. 2 and 3). These data suggest that NPe6–PDT-induced apoptosis is initiated at the level of mitochondria through a caspase-9-dependent intrinsic pathway.

In conclusion, our results demonstrated that NPe6–PDT induced immediate generation of ROS and the photodynamically produced ROS caused a rapid destruction of lysosomes, leading to release of

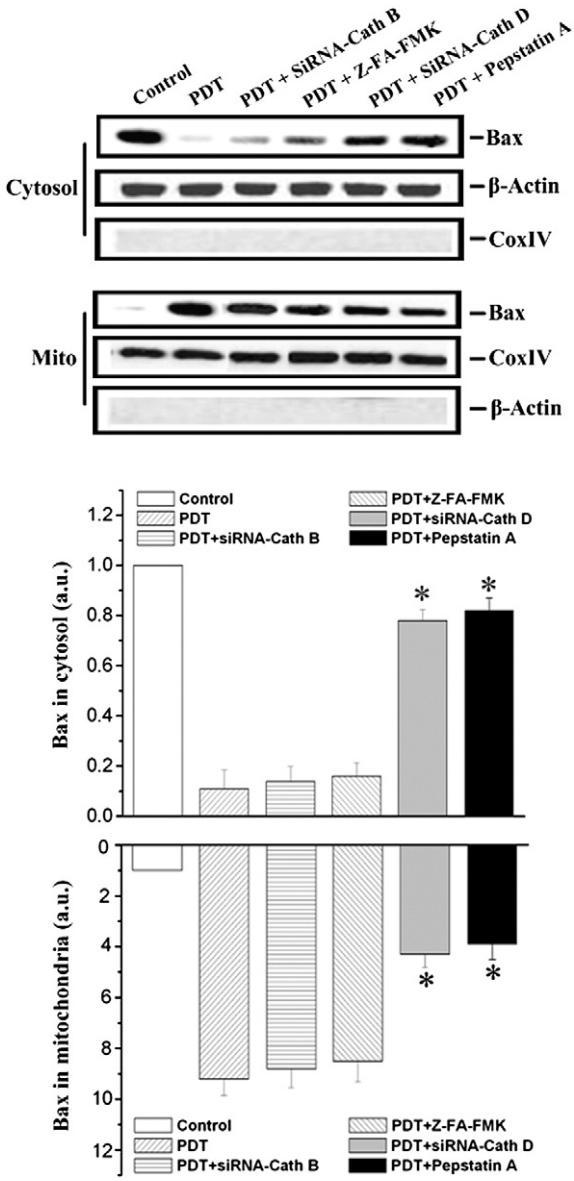


**Fig. 6.** Effects of inhibiting cathepsins on Bax translocation to mitochondria. The samples were treated as indicated. Cell lysates were subjected to immunoblotting. β-Actin and CoxIV were used as loading controls. Densitometric results of three separate blots were used for quantitative analysis. For densitometry, values were normalized according to the control sample lanes, which were arbitrarily set as 1; data represent means ± SD; $^{*}p<0.05$ versus PDT group.

cathepsins. Then the following spatiotemporal sequence of cellular events was observed during cell apoptosis: activation of Bax, loss of $\Delta\Psi_m$, cytochrome *c* release, and activation of caspase-9/-3. Importantly, Bax activation was proved to be a crucial event for the mitochondrial apoptotic pathway of apoptosis induced by lysosomal photodamage.

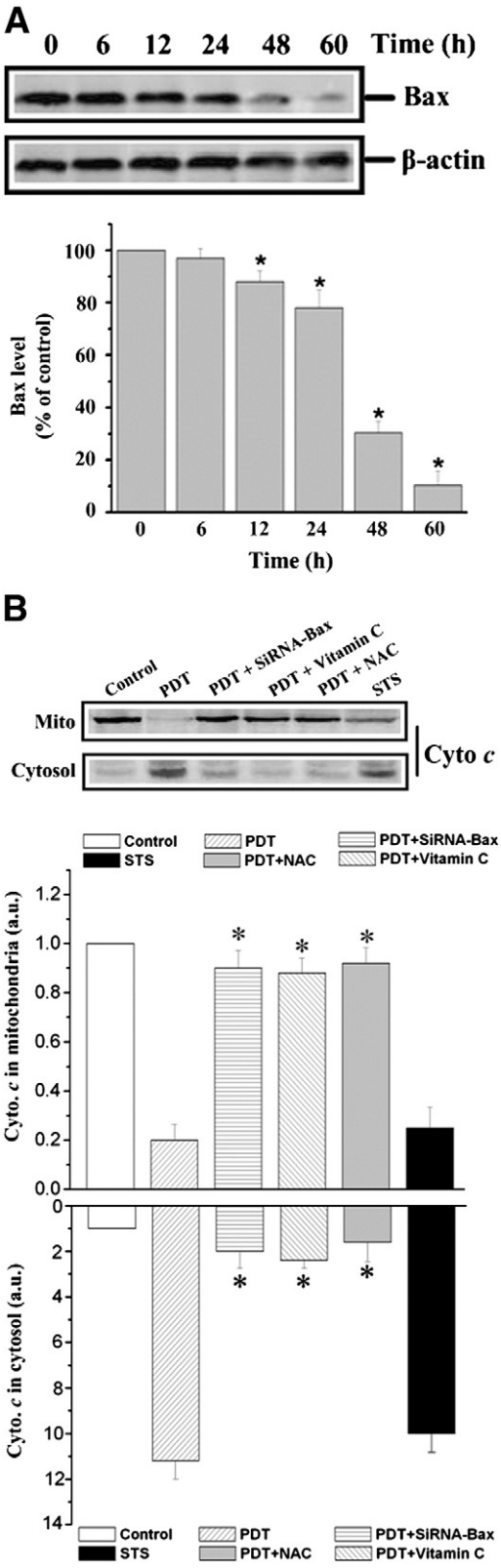


**Fig. 7.** Effects of suppressing Bax on cell apoptosis. (A) Western blot analysis for Bax expression. Bax expression decreased with time in ASTC-a-1 cells transfected with siRNA-Bax. Densitometric results of three separate blots were used for quantitative analysis. For densitometry, values were normalized according to the sample lanes at 0 h, which were arbitrarily set as 1; data represent means ± SD; $^{*}p<0.05$ versus control sample (0 h). (B) Effects of silencing Bax on cytochrome *c* release. (C) Caspase-9 activation. (D) Caspase-3 activation. The samples were treated as indicated. Cell lysates were subjected to immunoblotting. The experiments with STS treatment were used as positive controls; vitamin C and NAC were used to scavenge ROS; β-actin served as a loading control. For (B) to (D), densitometric results of three separate blots were used for quantitative analysis. For densitometry, values were normalized according to the control sample lanes, which were arbitrarily set as 1; data represent means ± SD; $^{*}p<0.05$ versus PDT group. (E) Effects of suppressing Bax on cell apoptosis induced by NPe6–PDT. Cells were treated as indicated. Apoptosis was measured by flow cytometry. Data displayed here are representatives of three separate experiments. The data show that knockdown of Bax attenuates NPe6–PDT-induced apoptosis.

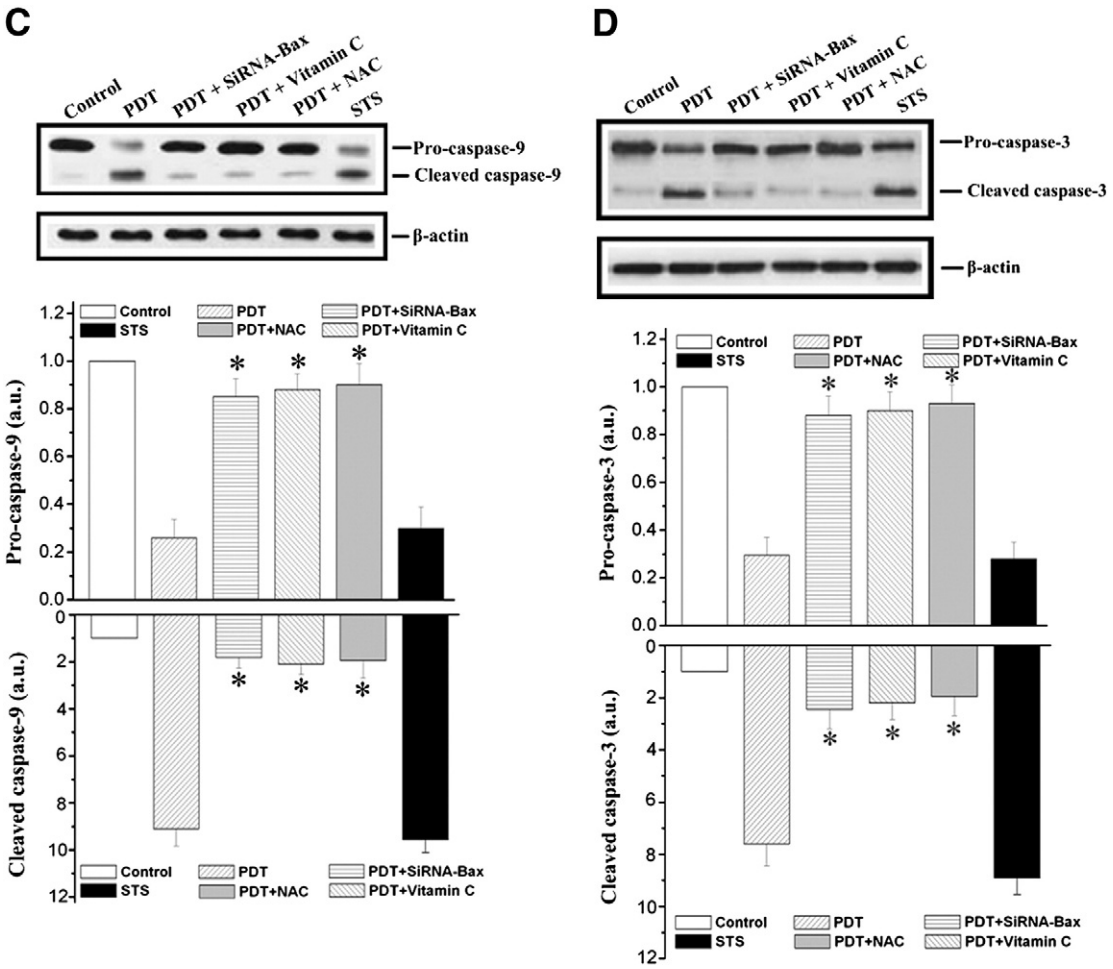


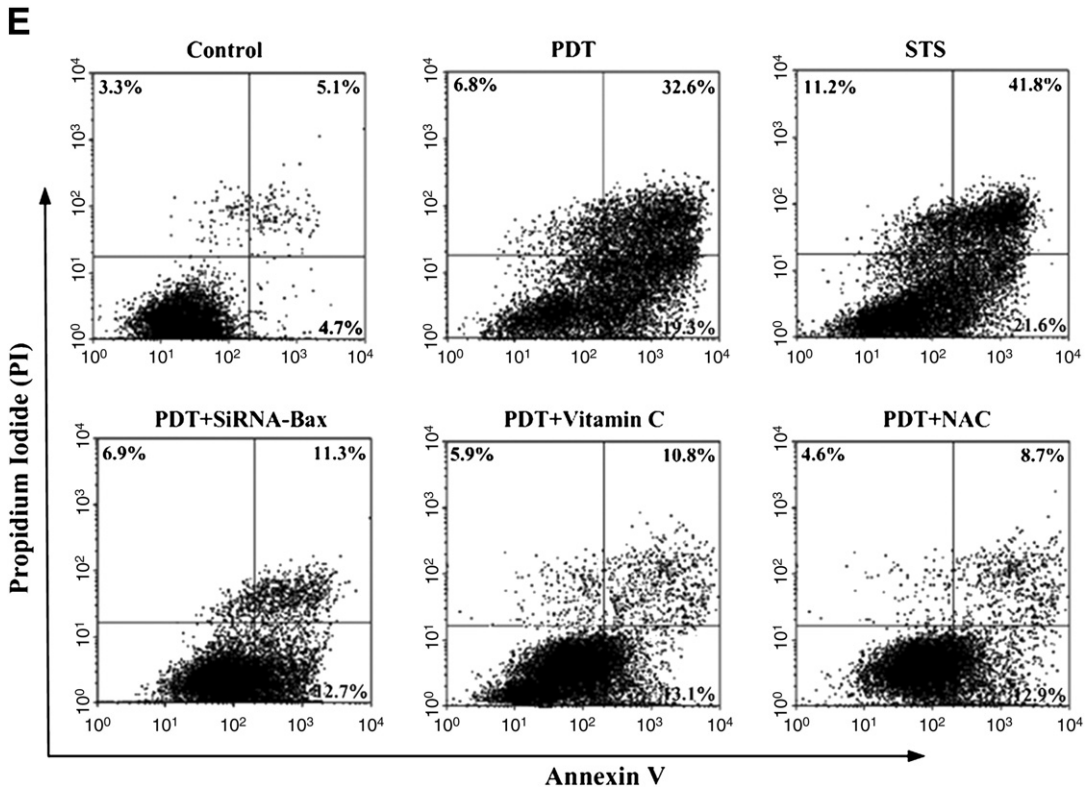


**Fig. 7** (*continued*).

## Acknowledgments

We thank Dr. M. Miura (RIKEN Brain Science Institute, Wako, Japan) for kindly providing pSCAT9 and pSCAT3 plasmids, Dr. G.J. Gores (Center for Basic Research in Digestive Diseases, Molecular Medicine Program, Mayo Clinic, Rochester, MN, USA) for kindly providing the pCyt. *c*-GFP plasmid, and Dr. R.J. Youle (National Institutes of Heath, Bethesda, MD, USA) for kindly providing the pCFP-Bax plasmid. We thank Dr. Wei R. Chen for discussion and comments. This research is supported by the National Basic Research Program of China (2011CB910402; 2010CB732602), the Program for Changjiang Scholars and Innovative Research Team in University (IRT0829), and the National Natural Science Foundation of China (30870676; 30870658).

## Appendix A. Supplementary data

Supplementary data to this article can be found online at doi:10.1016/j.freeradbiomed.2011.03.042.

## References

[1] Almeida, R. D.; Manadas, B. J.; Carvalho, A. P.; Duarte, C. B. Intracellular signaling mechanisms in photodynamic therapy. *Biochim. Biophys. Acta* **1704:**59–86; 2004.
[2] Buytaert, E.; Dewaele, M.; Agostinis, P. Molecular effectors of multiple cell death pathways initiated by photodynamic therapy. *Biochim. Biophys. Acta* **1776:** 86–107; 2007.
[3] Celli, J. P.; Spring, B. Q.; Rizvi, I.; Evans, C. L.; Samkoe, K. S.; Verma, S.; Pogue, B. W.; Hasan, T. Imaging and photodynamic therapy: mechanisms, monitoring, and optimization. *Chem. Rev.* **110:**2795–2838; 2010.
[4] Teiten, M. H.; Bezdetnaya, L.; Morliere, P.; Santus, R.; Guillemin, F. Endoplasmic reticulum and Golgi apparatus are the preferential sites of Foscan localisation in cultured tumour cells. *Br. J. Cancer* **88:**146–152; 2003.
[5] Morris, R. L.; Azizuddin, K.; Lam, M.; Berlin, J.; Nieminen, A. L.; Kenney, M. E.; Samia, A. C.; Burda, C.; Oleinick, N. L. Fluorescence resonance energy transfer reveals a binding site of a photosensitizer for photodynamic therapy. *Cancer Res.* **63:**5194–5197; 2003.
[6] Usuda, J.; Chiu, S. M.; Murphy, E. S.; Lam, M.; Nieminen, A. L.; Oleinick, N. L. Domain-dependent photodamage to Bcl-2: a membrane anchorage region is needed to form the target of phthalocyanine photosensitization. *J. Biol. Chem.* **278:** 2021–2029; 2003.
[7] Kessel, D.; Luo, Y.; Deng, Y.; Chang, C. K. The role of subcellular localization in initiation of apoptosis by photodynamic therapy. *Photochem. Photobiol.* **65:**422–426; 1997.
[8] Noodt, B. B.; Berg, K.; Stokke, T.; Peng, Q.; Nesland, J. M. Different apoptotic pathways are induced from various intracellular sites by tetraphenylporphyrins and light. *Br. J. Cancer* **79:**72–81; 1999.
[9] Kessel, D.; Luguya, R.; Vicente, M. G. Localization and photodynamic efficacy of two cationic porphyrins varying in charge distributions. *Photochem. Photobiol.* **78:** 431–435; 2003.
[10] Oleinick, N. L.; Morris, R. L.; Belichenko, I. The role of apoptosis in response to photodynamic therapy: what, where, why, and how. *Photochem. Photobiol. Sci.* **1:** 1–21; 2002.
[11] Moan, J.; Berg, K. The photodegradation of porphyrins in cells can be used to estimate the lifetime of singlet oxygen. *Photochem. Photobiol.* **53:**549–553; 1991.
[12] Kessel, D.; Luo, Y.; Mathieu, P.; Reiners Jr., J. J. Determinants of the apoptotic response to lysosomal photodamage. *Photochem. Photobiol.* **71:**196–200; 2000.
[13] Reiners Jr., J. J.; Caruso, J. A.; Mathieu, P.; Chelladurai, B.; Yin, X. M.; Kessel, D. Release of cytochrome c and activation of pro-caspase-9 following lysosomal photodamage involves Bid cleavage. *Cell Death Differ.* **9:**934–944; 2002.
[14] Caruso, J. A.; Mathieu, P. A.; Joiakim, A.; Leeson, B.; Kessel, D.; Sloane, B. F.; Reiners Jr., J. J. Differential susceptibilities of murine hepatoma 1c1c7 and Tao cells to the lysosomal photosensitizer NPe6: influence of aryl hydrocarbon receptor on lysosomal fragility and protease contents. *Mol. Pharmacol.* **65:** 1016–1028; 2004.
[15] Caruso, J. A.; Mathieu, P. A.; Reiners Jr., J. J. Sphingomyelins suppress the targeted disruption of lysosomes/endosomes by the photosensitizer NPe6 during photodynamic therapy. *Biochem. J.* **392:**325–334; 2005.
[16] Wan, Q.; Liu, L.; Xing, D.; Chen, Q. Bid is required in NPe6–PDT-induced apoptosis. *Photochem. Photobiol.* **84:**250–257; 2008.
[17] Green, D. R.; Kroemer, G. The pathophysiology of mitochondrial cell death. *Science* **305:**626–629; 2004.
[18] Antignani, A.; Youle, R. J. How do Bax and Bak lead to permeabilization of the outer mitochondrial membrane? *Curr. Opin. Cell Biol.* **18:**685–689; 2006.
[19] Adams, J. M.; Cory, S. Bcl-2-regulated apoptosis: mechanism and therapeutic potential. *Curr. Opin. Immunol.* **19:**488–496; 2007.
[20] Buytaert, E.; Callewaert, G.; Hendrickx, N.; Scorrano, L.; Hartmann, D.; Missiaen, L.; Vandenheede, J. R.; Heirman, I.; Grooten, J.; Agostinis, P. Role of endoplasmic reticulum depletion and multidomain proapoptotic BAX and BAK proteins in shaping cell death after hypericin-mediated photodynamic therapy. *FASEB J.* **20:** 756–758; 2006.
[21] Granville, D. J.; Shaw, J. R.; Leong, S.; Carthy, C. M.; Margaron, P.; Hunt, D. W.; McManus, B. M. Release of cytochrome c, Bax migration, Bid cleavage, and activation of caspases 2, 3, 6, 7, 8, and 9 during endothelial cell apoptosis. *Am. J. Pathol.* **155:**1021–1025; 1999.
[22] Bhowmick, R.; Girotti, A. W. Signaling events in apoptotic photokilling of 5-aminolevulinic acid-treated tumor cells: inhibitory effects of nitric oxide. *Free Radic. Biol. Med.* **47:**731–740; 2009.
[23] Chiu, S. M.; Xue, L. Y.; Usuda, J.; Azizuddin, K.; Oleinick, N. L. Bax is essential for mitochondrion-mediated apoptosis but not for cell death caused by photodynamic therapy. *Br. J. Cancer* **89:**1590–1597; 2003.
[24] Adams, J. M. Ways of dying: multiple pathways to apoptosis. *Genes Dev.* **17:** 2481–2495; 2003.
[25] Shi, Y. Mechanisms of caspase activation and inhibition during apoptosis. *Mol. Cell* **9:**459–470; 2002.
[26] Zhang, Y.; Xing, D.; Liu, L. PUMA promotes Bax translocation by both directly interacting with Bax and by competitive binding to Bcl-X L during UV-induced apoptosis. *Mol. Biol. Cell* **20:**3077–3087; 2009.
[27] Liu, L.; Xing, D.; Chen, W. R.; Chen, T.; Pei, Y.; Gao, X. Calpain-mediated pathway dominates cisplatin-induced apoptosis in human lung adenocarcinoma cells as determined by real-time single cell analysis. *Int. J. Cancer* **122:** 2210–2222; 2008.
[28] Liu, L.; Xing, D.; Chen, W. R. Micro-calpain regulates caspase-dependent and apoptosis inducing factor-mediated caspase-independent apoptotic pathways in cisplatin-induced apoptosis. *Int. J. Cancer* **125:**2757–2766; 2009.
[29] Xue, L. Y.; Chiu, S. M.; Oleinick, N. L. Photochemical destruction of the Bcl-2 oncoprotein during photodynamic therapy with the phthalocyanine photosensitizer Pc 4. *Oncogene* **20:**3420–3427; 2001.
[30] Ishisaka, R.; Utsumi, T.; Kanno, T.; Arita, K.; Katunuma, N.; Akiyama, J.; Utsumi, K. Participation of a cathepsin L-type protease in the activation of caspase-3. *Cell Struct. Funct.* **24:**465–470; 1999.
[31] Scorrano, L.; Oakes, S. A.; Opferman, J. T.; Cheng, E. H.; Sorcinelli, M. D.; Pozzan, T.; Korsmeyer, S. J. BAX and BAK regulation of endoplasmic reticulum $Ca^{2+}$: a control point for apoptosis. *Science* **300:**135–139; 2003.
[32] Zong, W. X.; Li, C.; Hatzivassiliou, G.; Lindsten, T.; Yu, Q. C.; Yuan, J.; Thompson, C. B. Bax and Bak can localize to the endoplasmic reticulum to initiate apoptosis. *J. Cell Biol.* **162:**59–69; 2003.
[33] Kagedal, K.; Johansson, A. C.; Johansson, U.; Heimlich, G.; Roberg, K.; Wang, N. S.; Jurgensmeier, J. M.; Ollinger, K. Lysosomal membrane permeabilization during apoptosis—involvement of Bax? *Int. J. Exp. Pathol.* **86:**309–321; 2005.
[34] Feldstein, A. E.; Werneburg, N. W.; Li, Z.; Bronk, S. F.; Gores, G. J. Bax inhibition protects against free fatty acid-induced lysosomal permeabilization. *Am. J. Physiol.* **290:**G1339–G1346; 2006.
[35] Walensky, L. D.; Pitter, K.; Morash, J.; Oh, K. J.; Barbuto, S.; Fisher, J.; Smith, E.; Verdine, G. L.; Korsmeyer, S. J. A stapled BID BH3 helix directly binds and activates BAX. *Mol. Cell* **24:**199–210; 2006.
[36] Willis, S. N.; Fletcher, J. I.; Kaufmann, T.; van Delft, M. F.; Chen, L.; Czabotar, P. E.; Ierino, H.; Lee, E. F.; Fairlie, W. D.; Bouillet, P.; Strasser, A.; Kluck, R. M.; Adams, J. M.; Huang, D. C. Apoptosis initiated when BH3 ligands engage multiple Bcl-2 homologs, not Bax or Bak. *Science* **315:**856–859; 2007.
[37] Uren, R. T.; Dewson, G.; Chen, L.; Coyne, S. C.; Huang, D. C.; Adams, J. M.; Kluck, R. M. Mitochondrial permeabilization relies on BH3 ligands engaging multiple prosurvival Bcl-2 relatives, not Bak. *J. Cell Biol.* **177:**277–287; 2007.
[38] Bidere, N.; Lorenzo, H. K.; Carmona, S.; Laforge, M.; Harper, F.; Dumont, C.; Senik, A. Cathepsin D triggers Bax activation, resulting in selective apoptosis-inducing factor (AIF) relocation in T lymphocytes entering the early commitment phase to apoptosis. *J. Biol. Chem.* **278:**31401–31411; 2003.
[39] Castino, R.; Bellio, N.; Nicotra, G.; Follo, C.; Trincheri, N. F.; Isidoro, C. Cathepsin D–Bax death pathway in oxidative stressed neuroblastoma cells. *Free Radic. Biol. Med.* **42:**1305–1316; 2007.
[40] Chipuk, J. E.; Kuwana, T.; Bouchier-Hayes, L.; Droin, N. M.; Newmeyer, D. D.; Schuler, M.; Green, D. R. Direct activation of Bax by p53 mediates mitochondrial membrane permeabilization and apoptosis. *Science* **303:**1010–1014; 2004.
[41] Chipuk, J. E.; Bouchier-Hayes, L.; Kuwana, T.; Newmeyer, D. D.; Green, D. R. PUMA couples the nuclear and cytoplasmic proapoptotic function of p53. *Science* **309:** 1732–1735; 2005.
[42] Gao, G.; Dou, Q. P. N-terminal cleavage of bax by calpain generates a potent proapoptotic 18-kDa fragment that promotes bcl-2-independent cytochrome C release and apoptotic cell death. *J. Cell. Biochem.* **80:**53–72; 2000.
[43] Cartron, P. F.; Oliver, L.; Juin, P.; Meflah, K.; Vallette, F. M. The p18 truncated form of Bax behaves like a Bcl-2 homology domain 3-only protein. *J. Biol. Chem.* **279:** 11503–11512; 2004.
[44] Dolmans, D. E.; Fukumura, D.; Jain, R. K. Photodynamic therapy for cancer. *Nat. Rev. Cancer* **3:**380–387; 2003.
[45] Castano, A. P.; Mroz, P.; Hamblin, M. R. Photodynamic therapy and anti-tumour immunity. *Nat. Rev. Cancer* **6:**535–545; 2006.